Chapter 9

Model Fitting to Power-Plant Steel Data

9.1 Data and fitting procedure

The output from the BN measurement software is a text file containing only the forward and reverse RMS noise data. From the BN unit control software, it was known that the applied current amplitude was ± 0.7 A. A program was written to extract the two sets of data and assign current values to them, assuming that BN data points were acquired at equally spaced intervals of current. It was further assumed, as in Chapter 5, that the current was proportional to the applied field experienced by the domain walls. Models 1 and 2 were fitted using the programs described in the Appendix.

9.2 Results

Figure 9.1–Figure 9.6 show examples of fitting using Model 1 and Model 2. Both models give a close fit, although Model 2 is rather better at correctly fitting the leading edge. Table 9.1 gives the errors calculated by the programs for all the data sets examined. The mean error of all the data sets, shown in the final row of the table, is smallest for Model 2 and largest for empirical fitting. The difference between the goodness of fit of Model 1 and Model 2 is less pronounced than for the data fitted in Chapter 5. The double peaks in those data increase the difficulty of fitting using a model which is physically

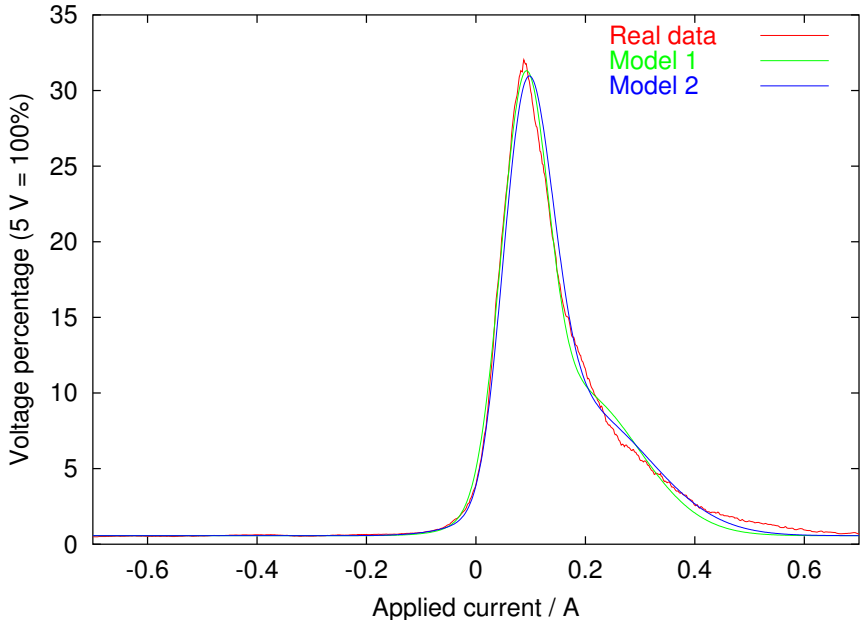

Figure 9.1: $2\frac{1}{4}$Cr1Mo steel, 500°C, 8 h

inaccurate, whereas a single peak with a slope change can be approximated more easily even by empirical fitting.

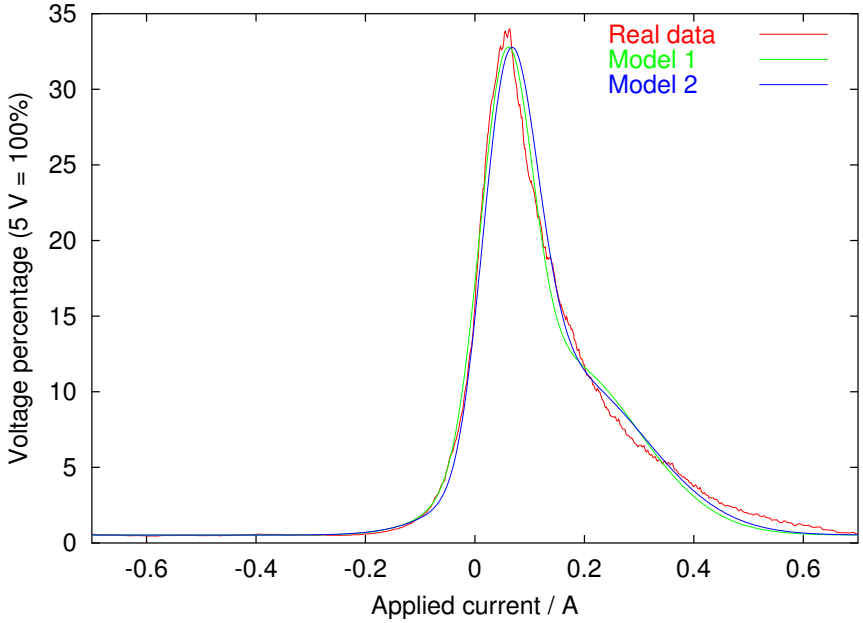

Figure 9.2: $2\frac{1}{4}$Cr1Mo steel, 600°C, 8 h

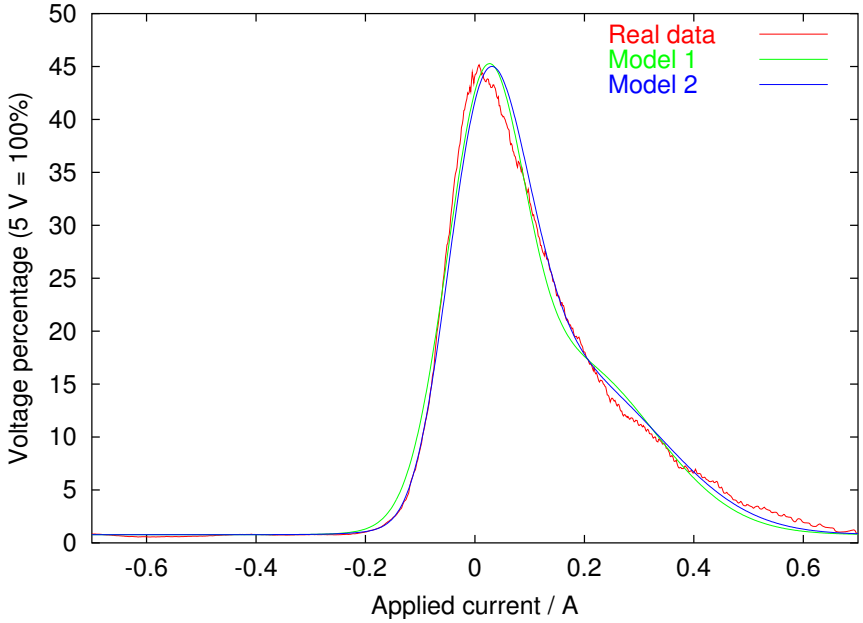

Figure 9.3: $2\frac{1}{4}$Cr1Mo steel, 700°C, 8 h

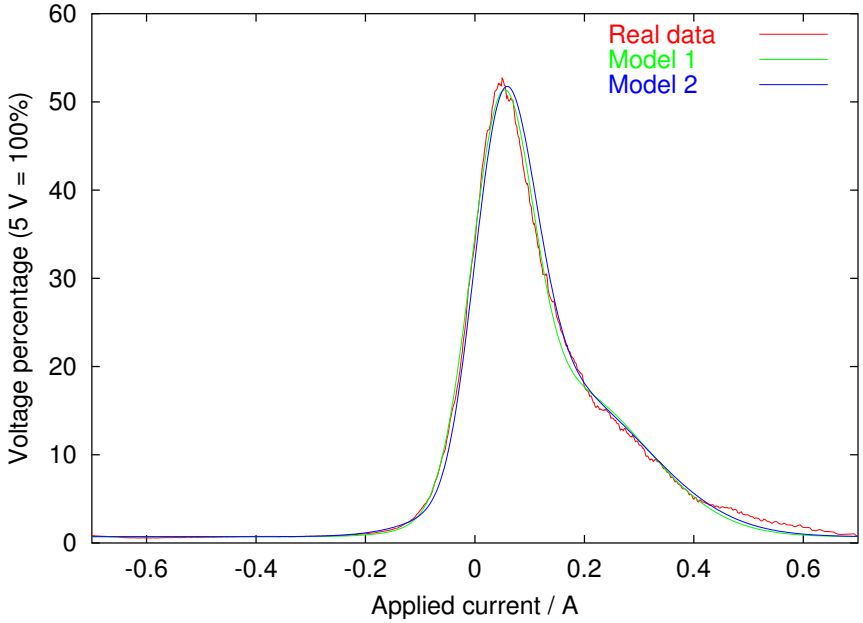

Figure 9.4: $2\frac{1}{4}$Cr1Mo steel, 600°C, 256 h

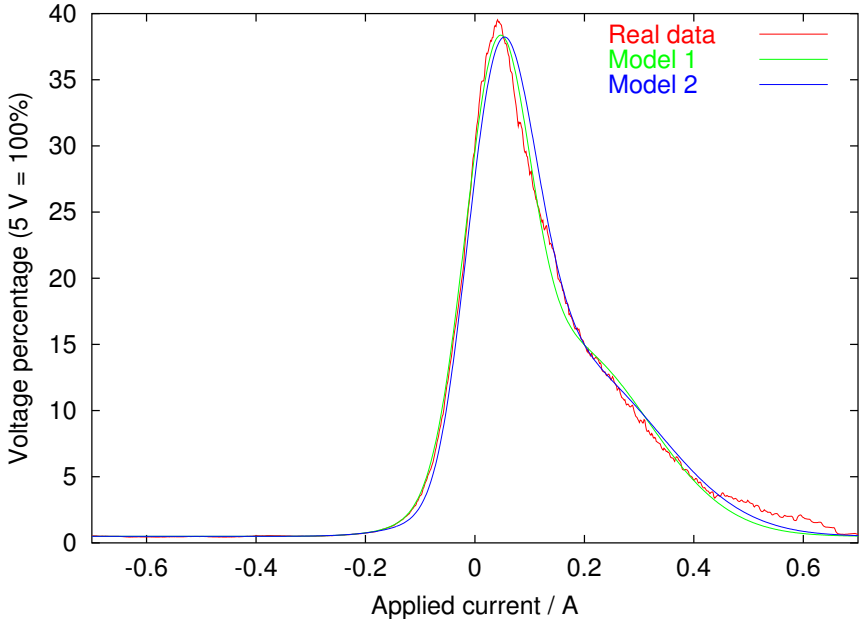

Figure 9.5: $2\frac{1}{4}$Cr1Mo steel, 600°C, 512 h

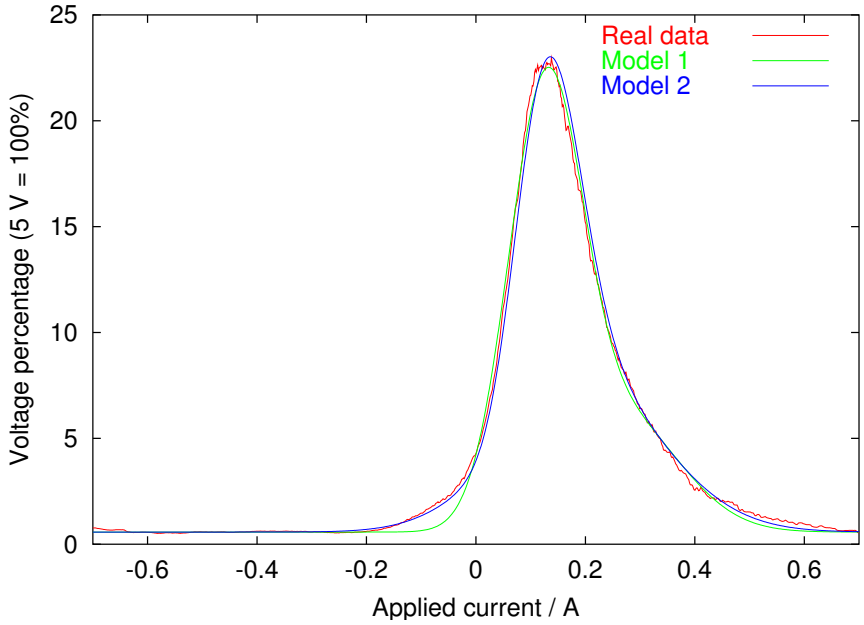

Figure 9.6: 11Cr1Mo wt. % steel, 550°C, 2347 h

9.3 Fitting parameters

9.3.1 Comparison of Model 1 and Model 2

The Model 2 parameters $e^{<x>} + S_b$ and $< S >_2$ are plotted against tempering time in Figure 9.7 and Figure 9.8. These characterise the average pinning strengths of the log-normal and normal distributions respectively. The $e^{<x>} + S_b$ values are divided into clear bands based on tempering temperature. Within the 500°C and 600°C bands, the values decrease with increasing time. The relationship between $< S >_2$, temperature and time is not so clear-cut, but the trends seem similar.

For comparison, the Model 1 fitting parameters $< S >_1$ and $< S >_2$ were also plotted against tempering time, giving very similar results. As discussed above, because of the lack of a distinct second peak, it is likely that Model 1 could be used in place of Model 2 to fit these data without a great loss of accuracy.

Temperature /°C	Time / hours	Error (%)		
		Peak-fitting	Model 1	Model 2
$2\frac{1}{4}$Cr1Mo steel				
As-quenched		4.09	4.44	4.23
500	1	6.03	5.69	4.67
500	2	8.40	5.19	4.20
500	4	7.32	4.97	4.01
500	8	6.57	6.11	5.19
500	16	6.41	6.12	5.40
500	32	6.60	6.22	4.41
500	256	7.48	7.33	6.03
500	512	7.23	6.92	5.94
600	4	6.05	5.89	6.71
600	8	7.87	7.51	6.71
600	16	4.74	4.23	4.37
600	32	8.76	8.53	9.90
600	64	5.30	5.21	4.36
600	128	4.56	4.27	3.73
600	256	5.05	4.60	3.56
600	512	6.10	5.75	5.09
700	1	6.97	6.14	5.42
700	2	4.82	3.75	3.03
700	4	4.30	3.80	3.50
700	8	7.34	7.13	5.10
11Cr1Mo steel				
550	2347	3.61	5.41	2.46
550	5849	4.44	4.12	4.64
550	16530	5.69	5.78	5.35
550	36191	5.23	5.40	4.58
Plain-carbon steel				
As-quenched		10.68	4.46	3.18
?	0.5	2.95	3.16	3.76
?	100	4.16	4.22	4.15
Mean				
		6.03	**5.44**	**4.77**

Table 9.1: Fitting errors of empirical peak-fitting, Model 1 and Model 2

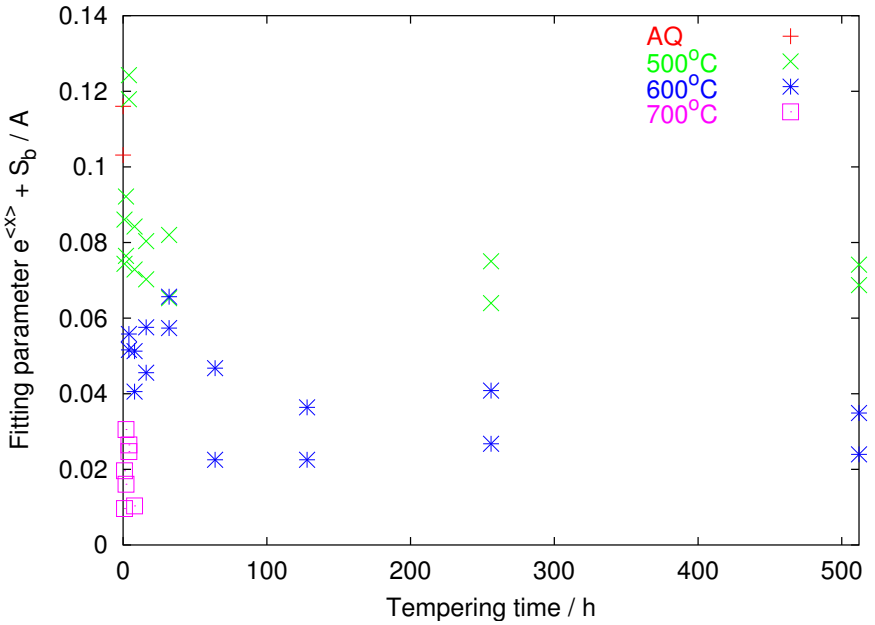

Figure 9.7: $e^{<x>} + S_b$ versus tempering time for Model 2, $2\frac{1}{4}$Cr1Mo steel.

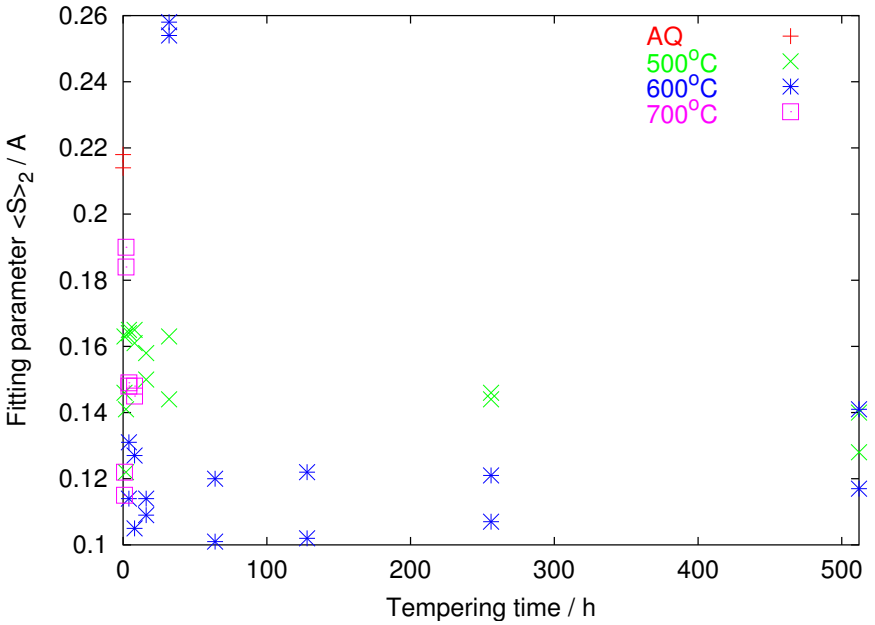

Figure 9.8: $< S >_2$ versus tempering time for Model 2, $2\frac{1}{4}$Cr1Mo steel.

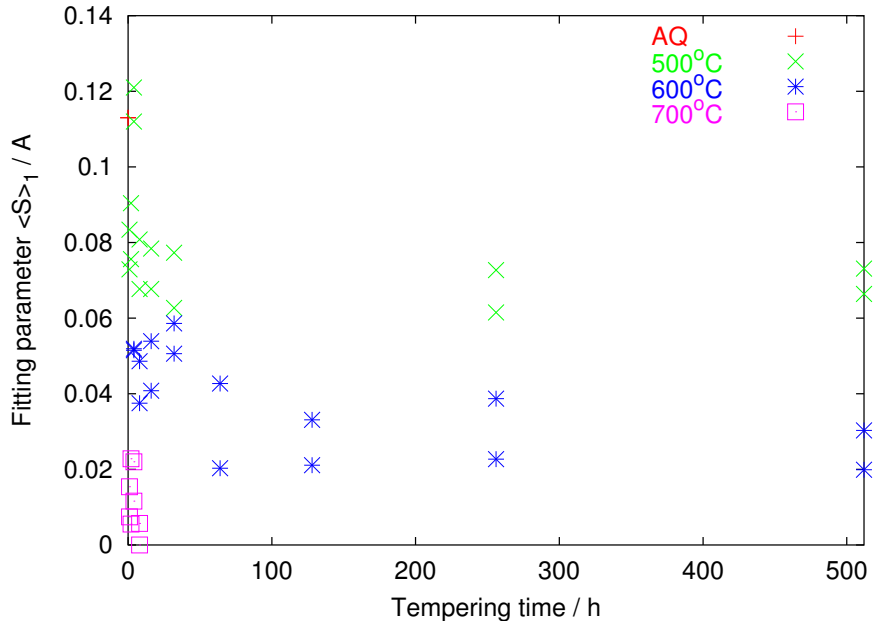

Figure 9.9: $< S >_1$ versus tempering time for Model 1, $2\frac{1}{4}$Cr1Mo steel.

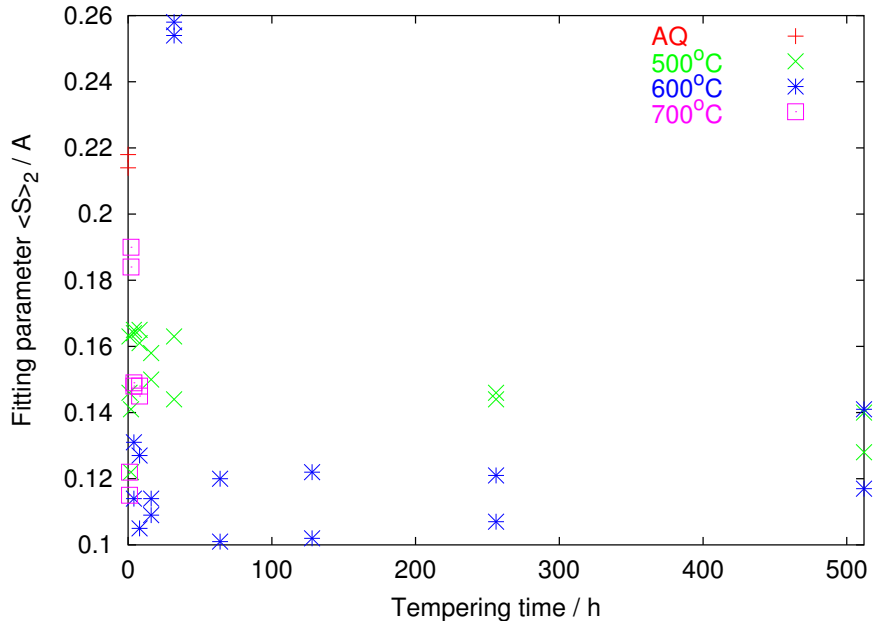

Figure 9.10: $< S >_2$ versus tempering time for Model 1, $2\frac{1}{4}$Cr1Mo steel.

9.3.2 Model 2 parameter variations with Larson-Miller parameter

The combination $e^{<x>} + S_b$ is plotted against the Larson-Miller parameter P in Figure 9.11. This is very similar in appearance to Figure 8.18, with a monotonic decrease in $e^{<x>} + S_b$ with P for all the $2\frac{1}{4}$Cr1Mo samples. The 11Cr1Mo samples have higher $e^{<x>} + S_b$ values than the $2\frac{1}{4}$Cr1Mo. $< S >_2$ decreases with P at short times, then increases again at longer times (Figure 9.12).

A_1 and A_2 both increase monotonically with increasing P in the $2\frac{1}{4}$Cr1Mo steel samples. The 11Cr1Mo values fall below these curves. A_2 has around half the value of A_1.

The distribution widths Δx and ΔS_2, shown in Figure 9.15 and Figure 9.16 respectively, tend to higher values at higher P, but there is more scatter than for A_1, A_2 and $e^{<x>} + S_b$.

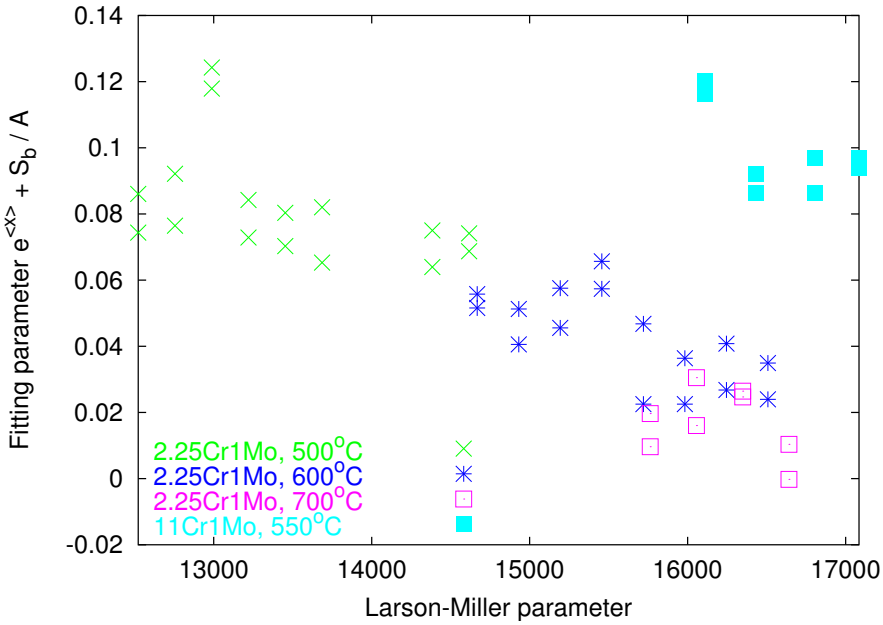

Figure 9.11: $e^{<x>} + S_b$ versus Larson-Miller parameter.

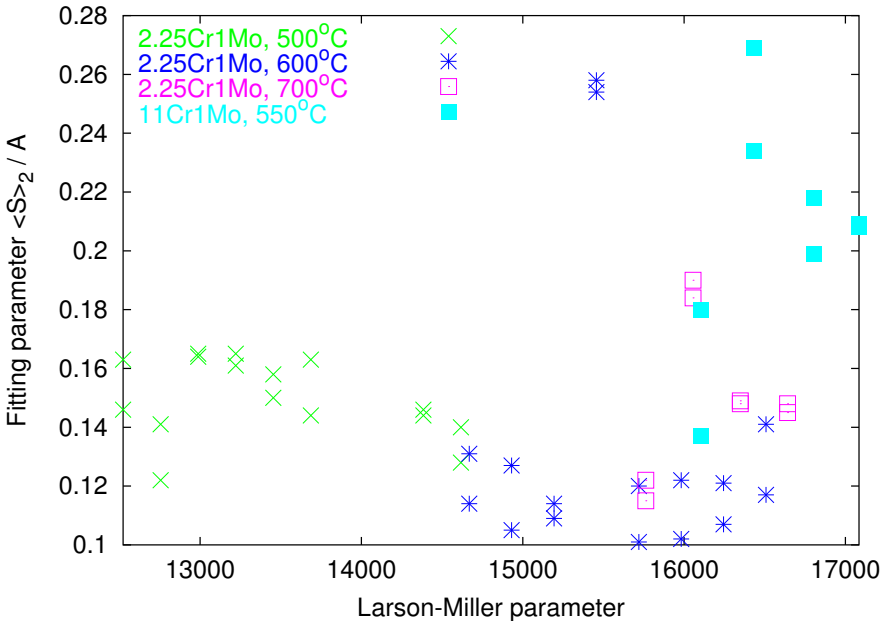

Figure 9.12: $< S >_2$ versus Larson-Miller parameter.

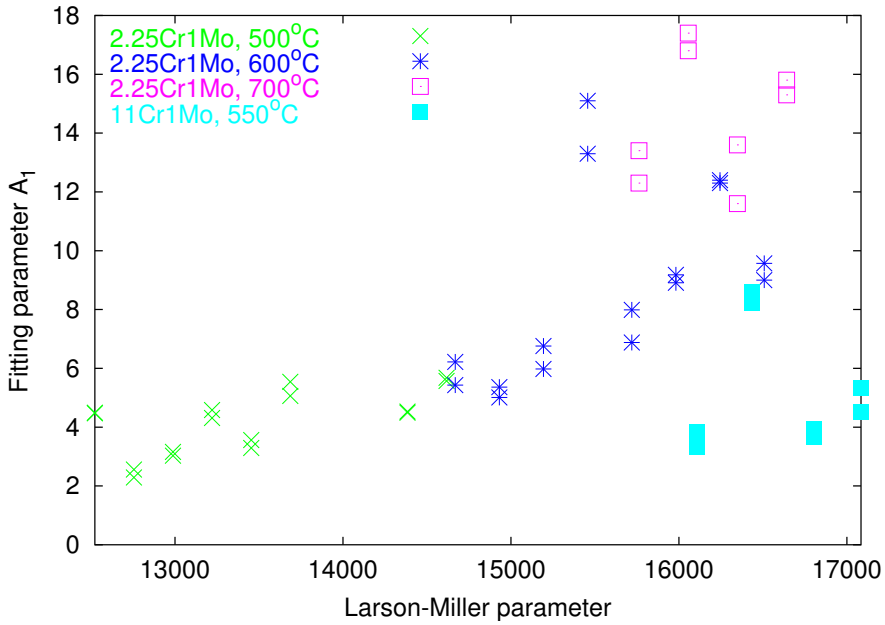

Figure 9.13: A_1 versus Larson-Miller parameter.

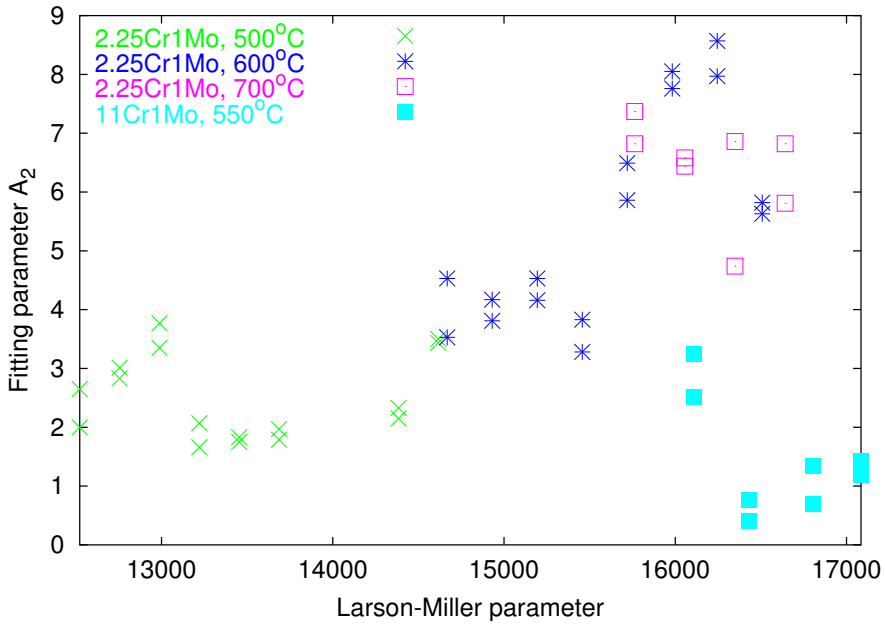

Figure 9.14: A_2 versus Larson-Miller parameter.

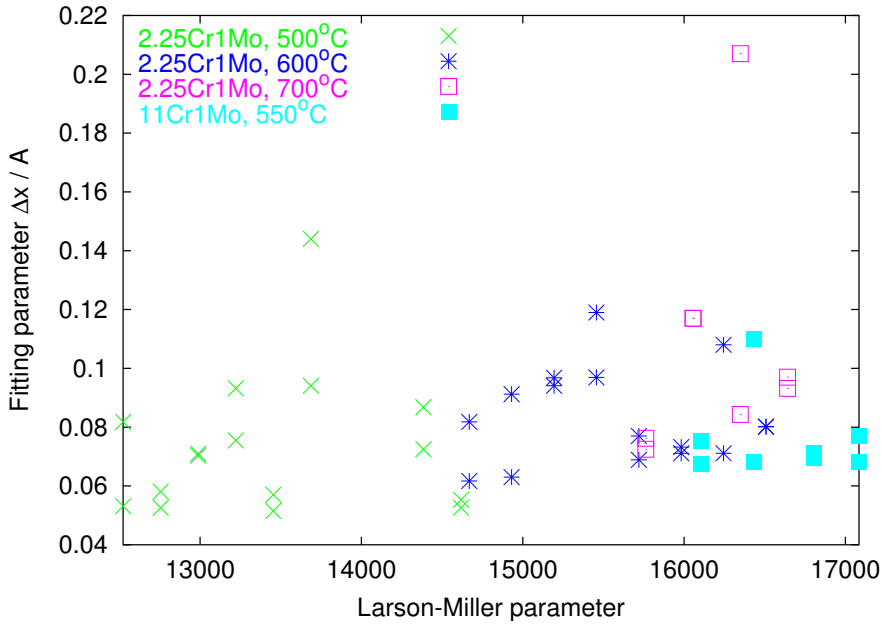

Figure 9.15: Δx versus Larson-Miller parameter.

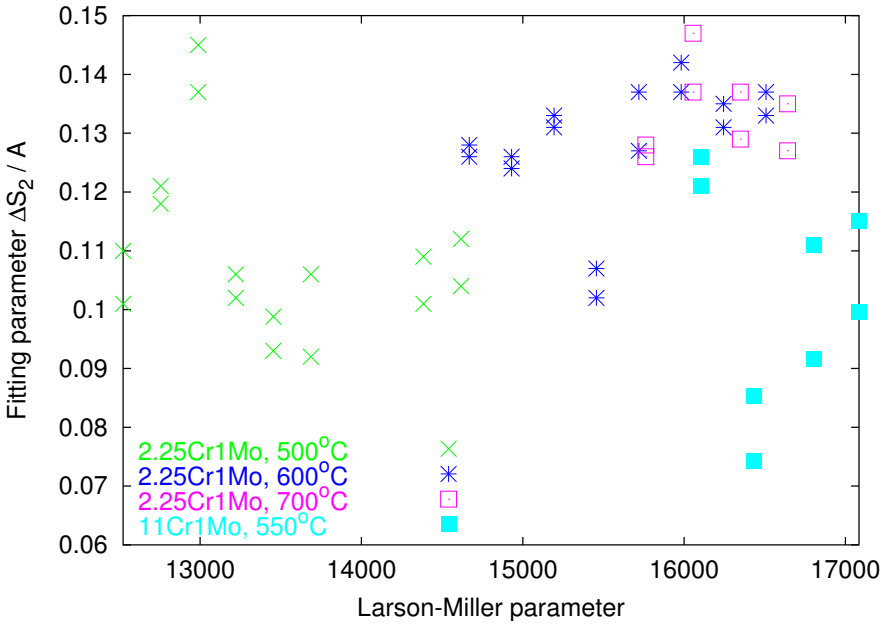

Figure 9.16: ΔS_2 versus Larson-Miller parameter.

9.4 Discussion

9.4.1 Relationship of fitting parameters to microstructure

It was seen in Chapter 6 that $2\frac{1}{4}$Cr1Mo steel samples tempered at 700°C underwent rapid microstructural coarsening and softening, but at 500 and 600°C, changes were much more gradual. Despite these differences, if the Larson-Miller parameter is used to combine temperature and time conditions, it can be seen that the BN model parameters from this steel fall into the same regime of behaviour. In particular, there is a very clear relationship between $e^{<x>} + S_b$ and the Larson-Miller parameter; this accurately replicates the relationship between peak position and P seen in Chapter 8. This large peak is believed to correspond to the lower-field peak observed by Moorthy *et al.* and attributed to interactions between domain walls and grain boundaries. If this is so, the results of Chapter 7 suggest that the gradual reduction of strain at grain boundaries during tempering reduces the strength of their interactions with domain walls. The lack of any clear changes in grain boundary character distribution during tempering at 600°C leads to the conclusion that the main changes are in magnetoelastic rather than magnetostatic energy, and are associated with changes in the dislocation density at grain boundaries. In as-quenched steel, adjacent martensitic laths within the same packet are separated by a highly strained boundary, but the misorientation between the laths is very small. Tempering reduces the dislocation density, and this decreases the strength and density of obstacles to domain wall motion.

No recrystallisation has been observed in any of the samples in this study. If the temperature and time were increased sufficiently to allow this, a different regime of BN behaviour, in which magnetostatic energy changes are important, may result.

The initial decrease of $< S >_2$ with tempering time may be related to the dissolution of M_3C and its replacement with fine, needlelike M_2X carbides, giving a reduction in pinning strength. The subsequent appearance and rapid growth of spheroidal M_7C_3 carbides and other coarse phases at longer times

increases $< S >_2$ again. It would be useful to repeat these experiments using BN apparatus which is capable of detecting double-peak behaviour to investigate the high-field region more fully.

The A parameters characterising the number of pinning sites show an unexpected monotonic increase with tempering time. It would be expected that the number of pinning sites from grain boundaries would fall as coarsening occurs, and the number of carbides may vary in a complex way during the precipitation sequence. The observed behaviour of A suggests that the model is not currently physically accurate in this respect. The width ΔS_2 does follow the expected behaviour of a carbide size distribution, increasing with tempering time as the carbide sizes become more varied, but Δx is more difficult to interpret.

The 11Cr1Mo steel BN parameters do not follow the same relationships as those of the $2\frac{1}{4}$Cr1Mo steel, although there is a suggestion in Figure 9.11 that its $e^{<x>} + S_b$ values may lie on a parallel line to the $2\frac{1}{4}$Cr1Mo steel values. However, more data, with a larger range of tempering conditions, would be needed to test this.

9.5 Conclusion

Model 2 fits these experimental data well, but almost as good a fit can be obtained using Model 1, possibly because the lack of a distinct second peak makes fitting easier. Clear relationships between the microstructural characteristics and the Model 2 parameters have been observed. From a comparison between microscopy, orientation measurements and modelling results, it has been concluded that the principal influence on magnetic behaviour in these samples is the reduction of the high levels of strain initially present in the quenched microstructure. However, it would be advisable to repeat the experiments using more suitable apparatus to check these conclusions.